RSC Advances

RSC Publishing

PAPER

View Article Online
View Journal | View Issue

Cite this: *RSC Adv.*, 2013, **3**, 21016

Highly stable PEGylated gold nanoparticles in water: applications in biology and catalysis†

Kamil Rahme,*[abc] Marie Therese Nolan,[d] Timothy Doody,[e] Gerard P. McGlacken,[d] Michael A. Morris,[ab] Caitriona O'Driscoll[e] and Justin D. Holmes[ab]

Received 17th April 2013
Accepted 20th August 2013

DOI: 10.1039/c3ra41873a

www.rsc.org/advances

Here we report the synthesis of well dispersed gold nanoparticles (Au NPs), with diameters ranging between 5 and 60 nm, in water and demonstrate their potential usefulness in catalysis and biological applications. Functionalised polyethylene glycol-based thiol polymers (mPEG-SH) were used to stabilise the pre-synthesised NPs. Successful PEGylation of the NPs was confirmed by Dynamic Light Scattering (DLS) and zeta potential measurements. PEG coating of the NPs was found to be key to their colloidal stability in high ionic strength media, compared to *bare* citrate-stabilised NPs. Our results show that PEG–Au NPs with diameters <30 nm were useful as catalysts in the homocoupling of arylboronic acids in water. Additionally, PEG–Au NPs were also shown to be stable in biological fluids, non-cytotoxic to B16.F10 and CT-26 cell lines and able to successfully deliver siRNA to CT-26 cells, achieving a significant reduction ($p < 0.05$) in the expression levels of luciferase protein; making these NPs attractive for further biological studies.

Introduction

The increasing progress of nanotechnology in the last few decades has made nanomaterials indispensable in many areas such as materials science, medicals, and cosmetics.[1–3] Nanoparticles (diameter 1–100 nm) exhibit particular properties that arise from quantum size effects and also from a high surface to volume ratio.[1,4,5] Their small size enables them to interact with biomolecules (such as enzymes, antibodies, DNA, proteins *etc.*) and cells.[6] As such, they are of appropriate dimensions for applications in nanobiotechnology and catalysis.[7–9] Noble metal nanoparticles, especially gold, are well known for their characteristic surface plasmon resonances which form the basis for many biological sensing and imaging applications.[1,4,10–13] Besides their potential applications in biology, the catalytic application of gold nanoparticles (Au NPs) in organic reactions has also been of considerable interest in recent years. Important transformations using Au catalysis, such as the selective oxidation of alcohols,[14–16] CO oxidation in the absence of H_2,[17–19] chemoselective reduction of nitroarenes,[20] and a wide variety of commercially important synthetic protocols have been studied exstensively.[21–23] Researchers have also shown that poly(2-aminothiophenol) (PATP)-supported Au NPs can be used in Suzuki–Miyaura cross-coupling reactions.[24] More recently, the homocoupling of arylhalides has been accomplished using a catalytic system comprising of Au NPs supported on a bifunctional periodic mesoporous organosilica.[25] Aryl boronic acids have also been homocoupled using Au on solid supports through apparent heterogeneous conditions. Homocoupling with high selectivity was achieved using Au supported on CeO_2.[26] The application of nanoparticles in biology and catalysis typically requires them to be well dispersed and stable in solution, which can be difficult due to their high surface energies.[27] Due to this instability, especially in the presence of salts, NPs can lose their size-dependent properties (catalytic, optical, magnetic *etc.*) caused by the high tendency of adhesion and aggregation.[28] Aggregation of nanoparticles is much more pronounced in solvents with high ionic strengths, *i.e.* biological fluids.[12] Therefore, the dispersion of NPs must be controlled to provide a better platform for the advancement of these materials in catalytic and biological applications.[29] In this manuscript we report the synthesis of stable colloidal Au NPs in water and under physiological conditions (0.15 M NaCl), achieved by attaching polyethylene glycol-based thiol polymers (mPEG-SH) as a stabilising ligand to the surfaces of Au NPs, *via* thiol linkages. PEG was the ligand of choice due to its ability to inhibit non-specific interactions with proteins in biological

[a]*Materials Chemistry and Analysis Group, Department of Chemistry and the Tyndall National Institute, University College Cork, Cork, Ireland*

[b]*Centre for Research on Adaptive Nanostructures and Nanodevices (CRANN), Trinity College Dublin, Dublin 2, Ireland*

[c]*Department of Sciences, Faculty of Natural and Applied Science, Notre Dame University (Louaize), Zouk Mosbeh, Lebanon. E-mail: kamil.rahme@ndu.edu.lb; Fax: +961 9 225164; Tel: +961 9 218950*

[d]*Organic and Pharmaceutical Chemistry Group, Department of Chemistry and Analytical and Biological Chemistry Research Facility, UCC, Cork, Ireland*

[e]*Pharmacodelivery group, School of Pharmacy, University College Cork, Cork, Ireland*

† Electronic supplementary information (ESI) available. See DOI: 10.1039/c3ra41873a

applications, as well as its compatibility with a diverse set of solvents (water, DMSO, THF *etc.*).[30,31] Further applications of Au NPs–PEG were demonstrated in the homocoupling of boronic acids in water.[32,33] Our data shows that the PEG–Au NPs, with diameters <30 nm, were useful as catalysts in the homocoupling of arylboronic acids in water, while PEG–Au NPs, with diameters of 60 nm, and Au NPs–citrate nanoparticles of different sizes (5, 15, 30 and 60 nm) had minimal catalytic efficiency. Moreover, the catalytic efficiency of 15 nm Au NPs–PEG_{10000}, expressed in term of the yield of pure 4-methoxyphenylboronic acid, was found to increase from 6 to 60% when the amount of Au NPs increased from 0.48 to 5 mol%. Finally, the PEG–Au NPs were complexed with siRNA and also tested for toxicity on B16.F10 and CT-26 cell lines, either alone or in the presence of siRNA, and for their aptitude in delivering siRNA to CT-26 cell lines.

Experimental

Chemicals and materials

Purified H_2O (resistivity $\approx$ 18.2 MΩ cm) was used as a solvent. All glassware was cleaned with aqua regia (3 parts of concentrated HCl and 1 part of concentrated HNO_3), rinsed with distilled water, ethanol, and acetone and oven-dried before use. Tetrachloroauric acid trihydrate ($HAuCl_4 \cdot 3H_2O$), sodium citrate ($C_6H_5Na_3O_7 \cdot 2H_2O$), sodium borohydride ($NaBH_4$) and ascorbic acid were purchased from Sigma Aldrich. Thiol terminated poly(ethylene glycol) methyl ether, $M_w = 2100$, 5400, 10 800 and 20 800 g mol^{-1} were purchased from Polymer Source®. All products were used as received.

Preparation and PEGylation of gold nanoparticles

Diameter of 5 ± 1.5 nm Au NPs. To an aqueous solution (150 mL) of $HAuCl_4 \cdot 3H_2O$ (0.25 mmol L^{-1}) was added 2.5 μmol of a 200 μM mPEG-SH (M_w = 10 800 g mol^{-1}) solution and the mixture was stirred vigorously. To this solution was added an ice cold solution of $NaBH_4$ in order to have a final concentration of 0.25 mmol L^{-1} $NaBH_4$. After addition of $NaBH_4$, an instantaneous colour change from pale yellow to deep red was noted. The Au NPs obtained with this procedure were approximately 5 ± 1.5 nm.

Diameter of ~15 ± 1.5 nm Au NPs. 150 mL of an aqueous solution of $HAuCl_4 \cdot 3H_2O$ (0.25 mmol L^{-1}) was heated to 95 °C with stirring. 0.53 mL of a 340 mmol L^{-1} sodium citrate aqueous solution was rapidly added. The colour of the solution changed from pale yellow to dark blue, and then to deep red-burgundy within about 8 min. Stirring and heating was maintained during 1.5 h after addition of sodium citrate. The heat was then removed and the solution was kept under stirring, until cooled to room temperature. The Au NPs obtained with this procedure were ~15 ± 1.5 nm.

Preparation of ~30 ± 4 nm and ~60 nm ± 8 nm Au NPs. For Au NPs, larger than 15 nm, a weak reducing agent ascorbic acid was used. For ~30 nm Au NPs, 150 mL of an aqueous solution of $HAuCl_4 \cdot 3H_2O$ (0.25 mmol L^{-1}) and 1 mmol L^{-1} sodium citrate was stirred vigorously. To this solution was added a volume of ascorbic acid in order to have a final concentration of 0.38 mmol L^{-1}. After addition of ascorbic acid the colour of the solution changed from pale yellow to dark blue, and then to deep red-burgundy in less than 1 min. Stirring and was maintained for 1 h. The Au NPs obtained were 30 ± 4 nm. By increasing the concentration of ascorbic acid to 1 mmol L^{-1}, added in 2 amounts (0.5 each), Au NPs ~60 nm ± 8 nm were obtained, we note that these Au NPs were less monodisperse.

Grafting of poly(ethylene glycol) ligands. Thiolated polyethylene glycol (mPEG-SH) was covalently grafted to the surface of the Au nanoparticles. A solution of mPEG-SH of the desired molecular weight was added to a solution of citrate-capped Au nanoparticles with stirring. The solution was stirred for ~1 h allowing citrate ligands to exchange with mPEG-SH. The excess mPEG-SH was removed *via* centrifugation at 15 000 rpm for about 45 min. Thiol groups are known to have a strong affinity for Au, resulting in covalent attachment of PEG to the Au nanoparticles. The resulting colloidal solutions were very stable for several months, as well as in high ionic strength solvents and biological fluids, furthermore they were able to undergo filtration and freeze drying.

UV-visible spectroscopy

Optical absorption spectra were obtained on a CARY UV-visible spectrophotometer with a xenon lamp (300–900 nm range, 0.5 nm resolution).

Dynamic light scattering and zeta potential measurements

The pristine solutions of Au and PEGylated Au nanoparticles, were diluted by 5 to 10 times depending on the initial concentration (absorption range 0.2–0.5) prior to dynamic light scattering (DLS) measurements. The measurements were undertaken with the Malvern instrument (Zetasizer Nano Series) at 25 °C using the default non-invasive back scattering (NIBS) technique with a detection angle of 173°. Three measurements were made per sample and the standard deviation (σ) was calculated, typically σ = 1–2 nm.

Transmission electron microscopy

Citrate and PEG-stabilised Au nanoparticles were placed on carbon-coated copper grids (Quantifoil, Germany) and dried over night in air, prior to transmission electron microscope (TEM) inspection. The samples were inspected using a JEOL JEM-2100 TEM operating at 200 kV. All the micrographs were recorded on a Gatan 1.35k × 1.04k × 12 bit ES500W CCD camera. TEM images were analysed using Image J software.

Scanning electron microscopy

Citrate and PEG-stabilised gold nanoparticles were deposited from solution on a silicon wafer and dried in air prior to inspection by scanning electron microscope (SEM). The samples were inspected using a FEI 630 NanoSEM equipped with an Oxford INCA energy dispersive X-ray (EDX) detector, operating at 5 kV.

General protocol for homocoupling: characterisation data

Synthesis of biphenyl.

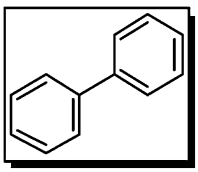

In a round bottom flask (100 mL) equipped with a condenser and magnetic stirrer bar, phenylboronic acid (2 mmol) and NaOH (8 mmol) were mixed with 15 nm Au NP–PEG_{2000} (2 mol%) in H_2O (40 mL). The resulting mixture was stirred at 80 °C for 48 h. The crude reaction mixture was then extracted with ethyl acetate (3 × 20 mL). The organic layers were combined and washed with 10% aqueous NaOH solution, dried with $MgSO_4$, filtered and concentrated under reduced pressure to afford the pure product (67 mg, 44%) as a white solid, m.p. 67–68 °C (ref. 2 67–69 °C); λ_{max}/cm^{-1} (KBr): 3034, 1943, 1569, 1480, 1429, 729, 696; δ_H (300 MHz) 7.61–7.57 [4H, m], 7.46–7.41 [4H, m], 7.39–7.31 [2H, m]; δ_C ($CDCl_3$, 75.5 MHz) 141.26, 128.8, 127.3, 127.2.

Synthesis of 4,4′-dimethoxybiphenyl.

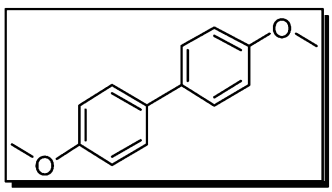

In a round bottom flask (100 mL) equipped with a condenser and magnetic stirrer bar, *para*-methoxy boronic acid (1 mmol) and NaOH (2 mmol) were mixed with 15 nm Au NP–PEG_{10000} (5 mol%) in H_2O (25 mL). The resulting mixture was stirred at 80 °C for 22 h. The crude reaction mixture was then extracted with ethyl acetate (3 × 20 mL). The organic layers were combined and washed with 10% aqueous NaOH solution, dried with $MgSO_4$, filtered and concentrated under reduced pressure to afford the pure product (64.2 mg, 60%) as a white solid, m.p. 168–169 °C (ref. 3 168–170 °C); λ_{max}/cm^{-1} (KBr):[4] 2958, 1500, 1439, 1276, 1249, 1041; δ_H (300 MHz) 7.49–7.45 [4H, m], 6.98–6.93 [4H, m], 3.84 [6H, s]; δ_C ($CDCl_3$, 75.5 MHz) 158.7, 133.5, 127.7, 114.2, 55.4.

NMR spectroscopy (NMR)

NMR spectra were run in $CDCl_3$ using tetramethylsilane (TMS) as the internal standard. ^1H NMR spectra were recorded at 300 MHz on a Bruker AVANCE 300 spectrometer. ^{13}C NMR spectra were recorded at 75 MHz on a Bruker AVANCE 300 instrument.

Infra-red spectroscopy (IR)

IR spectra were recorded on a Perkin-Elmer FT-IR Paragon 1000 spectrophotometer. Solid samples were dispersed in potassium bromide and recorded as pressed discs.

Melting points

Melting points were measured in a Thomas Hoover Capillary Melting Point apparatus.

Dynamic light scattering and zeta potential measurements in the presence of biomolecules

Au–PEG particles were complexed with siRNA or siRNA : protamine at a molar ratio of 1 : 10. Samples were complexed for 1 h and subsequently diluted in either double distilled H_2O or in Dulbecco's modified eagle's medium without phenol red (Sigma-Aldrich) prior to DLS and zeta potential analysis. Measurements were performed using a Zetasizer Nano from Malvern instruments at 25 °C (back scattering at 173° NIBS default). The model used in the fitting procedure was provided by the instrument (using Mark Houwink parameters and cumulative fit). The standard deviation was calculated by performing three measurements on each sample.

Cell culture, cytotoxicity and *in vitro* siRNA knockdown

MTT cytotoxicity assay. The murine melanoma stably expressing pGL4 luc2 lentivirus, B16-F10-luc2 (Caliper Life Sciences, Hopkinton, MA) were routinely cultured in RPMI 1640 supplemented with 10% foetal bovine serum and grown in 5% CO_2 at 37 °C. Prior to cytotoxicity determination cells were seeded at a density of 4×10^4 cells in a 96-well plate and grown in complete media for 24 h. Cell viability was determined by the MTT assay which measures the reduction of MTT to formazan by mitochondrial reductase enzymes giving a purple colour. Au NPs alone and protamine condensed siRNA (50 nM) complexed with Au nanoparticles, were added to the cells and incubated for 4 h. The medium was removed and replaced with fresh complete medium containing MTT ((3-(4,5-dimethylthiazole-2-yl)-2,5-diphenyltetrazolium) bromide) (Sigma) at a working concentration of 0.5 mg mL^{-1}. After 4 h of incubation the cell culture medium was removed, and the formazan crystals produced were dissolved in 100 μL DMSO for 5 min at room temperature. Absorbance was read at a wavelength of 590 nm. A similar procedure described above was also performed on murine colon carcinoma cell line, CT26. All experiments were performed in triplicate.

In vitro siRNA knockdown

Cell culture and *in vitro* siRNA knockdown. The murine colon carcinoma cell line, CT26, was obtained from the American Type Culture Collection (ATCC). Cells were maintained in Dulbecco's modified Eagle medium (Sigma) supplemented with 10% fetal bovine serum (Sigma). Cells were grown in 5% CO_2 at 37 °C. For *in vitro* siRNA knockdown, cells were seeded, 24 h prior to transfection at a density of 5×10^4 cells in a 24 well plate. Cells were transfected with luciferase reporter plasmid, pGL3Luc (1 μg per well) complexed with Lipofectamine 2000 (3 μL μg^{-1} DNA) for 2 h. Cells were then washed twice with PBS prior to siRNA transfection. Luc GL3 siRNA (50 nM), was condensed with protamine (MR5 – mass ratio), and subsequently complexed with Au NP's (MR10) or Lipofectamine 2000

(1 μL μL^{-1} siRNA). Luc GL3 siRNA alone and non-silencing siRNA were used as control. After 4 h, complexes were removed and fresh medium was added to each well. Cells were incubated for a further 20 h and luciferase was determined using a luciferase assay kit (Promega) according to the manufacturer's instructions. Luciferase expression levels were normalised to cell protein content as determined by BCA (bicinchoninic acid) protein assay (Pierce). Experiments were carried out in triplicate.

Fluorescence microscopy

CT26 cells were seeded at a density of 5×10^4 per well on glass cover slips in a 24 well plate and grown for 24 h. Prior to addition of particles, cells were washed and fresh media was added. Fluorescently-labelled protamine condensed siRNA, complexed with Au NP's at MR 10, and control formulation (protamine condensed siRNA), were added to the cells and incubated for 20 h. The media was subsequently removed and the cells washed with cell scrub buffer (AMS Biotechnology). The cells were fixed for 15 min at room temperature in 3% paraformaldehyde (PFA). The coverslips were washed twice with 1× PBS at room temperature. Free aldehyde groups were quenched with 50 mM NH_4Cl solution at room temperature. Following two more washes with 1× PBS, the coverslips were mounted on glass slides. Association of the particles with cells was assessed by fluorescent detection of the labeled siRNA using a Nikon Eclipse TS100 inverted microscope equipped with fluorescein and DAPI filters and Metamorph version 6.1 software.

Results and discussion

Preparation and characterisation of PEG–Au NPs

Au NPs were synthesised with mean diameters of 5 ± 1.5 nm, 15 ± 1.5 nm, 30 ± 4 nm and 60 ± 8 nm in water by the controlled chemical reduction of a $HAuCl_4$ solution. Different reducing agents were used to produce Au NPs in this study; the strong reducing agent sodium borohydride ($NaBH_4$) was used at room temperature to produce Au NPs with a mean diameter of 5 nm; sodium citrate, a mild reducing agent, was used at high temperature to produce ~15 nm Au NPs, and finally ascorbic acid, a weak reducing agent, was used at room temperature to produce Au NPs with mean diameters of 30 and 60 nm.[34–37] The physical properties of the Au NPs synthesised were characterised using UV-visible spectroscopy and either TEM or SEM (Fig. 1). The UV-visible data clearly show that the NPs synthesised exhibited size dependent optical properties, resulting in a shift of the surface plasmon resonance (SPR) band from a wavelength of 514 to 534 nm, as the mean diameter of the Au NPs increased from 5 to 60 nm respectively.[4] TEM and SEM analysis of the NPs, utilising *Image J* software, showed a size polydispersity below 20%, with the exception of the 60 nm Au NPs (~30%). Electrostatically-stabilised NPs are very sensitive to changes in pH and ionic strength.[12,29,38] Therefore, to maintain an adequate dispersion of Au NPs in high ionic strength media, they were coated with the PEG-SH capping ligand directly after synthesis. The stability of the PEG–Au NPs under physiological conditions (0.157 mol L^{-1} NaCl), was monitored by UV-visible spectroscopy (Fig. 2) and the number of PEG-SH ligands needed to coat the surface of a Au NP of a particular diameter was estimated.[39] The grafting density was also determined by TGA and TEM.[39] Our data have shown that Au NPs–PEG hybrids were very stable when compared to *bare* citrate-stabilised Au NPs in the presence of NaCl (see ESI, Fig. S1†). Following the addition of salt to the citrate-stabilised Au NPs, the initial red colour of the colloidal solution immediately turned blue, due to a shift of the SPR peak at ~520 nm to 532 nm, with the immediate appearance of a second band at ~690 nm after 1 minute, attributed to a change in the dispersion of the Au NPs–citrate solution in the presence of NaCl (0.157 M). A further shift to higher wavelength, ~710 nm after 20 minutes, ~722 after about 1 hour and finally ~734 nm after 2 hours, was also observed. This continuous shift was accompanied by a decrease in the absorption of the overall UV-visible spectra over time (Fig. 2a), that can be attributed to citrate-stabilised Au NPs aggregation.[12,29,40] No nanoparticles were observed in solution after 3–4 hours and a black precipitate was detected visually after this time period (Fig. 2a). However, the PEG-stabilised Au NPs were only slightly affected by the addition of salt to the dispersion and no colour change of the solution was observed (Fig. S1†), due to their high stability in high ionic strength conditions. Fig. 2b shows the spectrum of Au NPs–PEG_{10000} before ($t = 0$), 1 minute, 3 and 24 hours after adding NaCl. The successful PEGylation of the Au NPs was also confirmed by DLS/zeta potential measurements in the presence of salt. Fig. 3a shows DLS analysis for 15 nm Au NPs functionalised with various mPEG-SH molecular weight ligands at different polymer concentrations. The mean diameter of the Au NPs was observed to increase with the PEG concentration in all cases. This increase was more pronounced as the length of the PEG capping ligand increased, *i.e.* Au NPs–citrate size increased from 19.8 to 41 nm when coated with PEG_{10000}. However, the size increase was less pronounced with the shorter PEG_{2000}, indicating that more polymer was grafted onto the Au NPs before reaching surface saturation (plateau). A similar trend was seen for the zeta potential measurements Fig. 3b. We note that TGA used in a previous study, also showed that the number of PEG ligands grafted on ~15 nm Au NPs increased when the PEG length decreased.[39] The hydrodynamic diameter increases with the PEG length inducing a thicker PEG layer which shields the surface charges, providing good stability.[12,29,39,40] In addition, the PEG–Au NPs did not aggregate significantly in the presence of NaCl and other salts. DLS/zeta combined with TEM analysis, provided full characterisation of the colloidal dispersion for further applications.

PEG–Au NPs catalytic efficiency

We initially tested *bare* 5, 15, 30 and 60 nm Au NPs–citrate as catalysts under Suzuki–Miyaura-type conditions. When bromobenzene, phenyl boronic acid and NaOH were heated in water (95–100 °C) the colour of the solution changed from red to blue, indicating that the citrate-stabilised Au NPs aggregated under these conditions. In all experiments, less than 2%

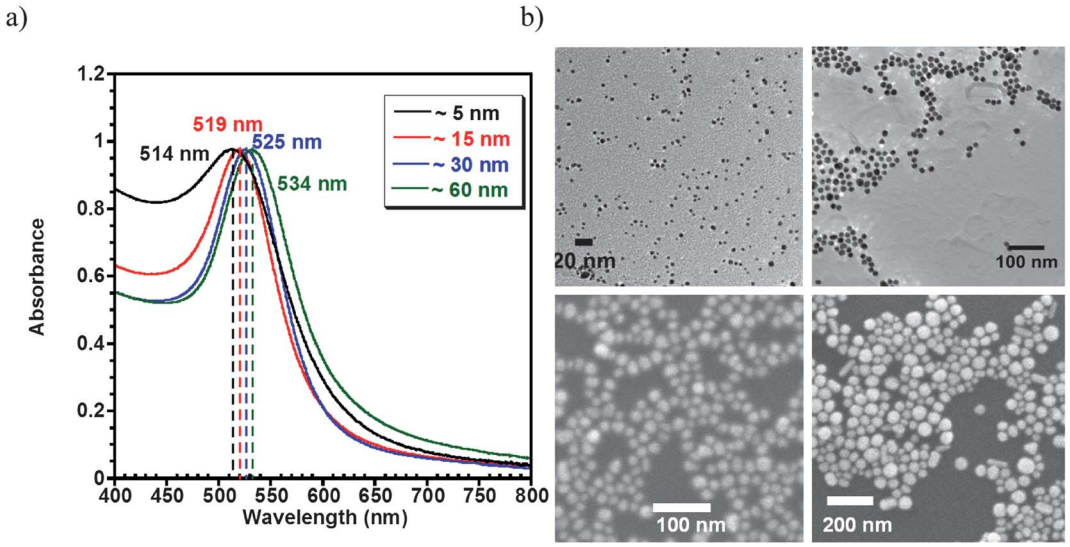

Fig. 1 (a) UV-visible spectra, and (b) TEM/SEM micrographs of the Au NPs–citrate with diameter ~5 nm (top left); ~15 nm (top right); 30 nm (bottom left) and 60 nm (bottom right) obtained in this study.

conversion to biaryl products was observed, similar results of about 2% conversion were also obtained in the absence of Au NPs, indicating that Au NPs–citrate has no catalytic efficiency under the above conditions. Similarly, Au NPs, with a mean diameter of 15nm and stabilised by PEG-SH 10800, were tested under Suzuki–Miyaura-type conditions. Again, we observed that a significant amount of starting materials remained unreacted as judged from analysis of the NMR spectra of our crude reaction mixture. However pure biphenyl was isolated in trace amounts (~2%, Scheme 1). To test if homocoupling rather than cross-coupling was occurring, we repeated the reaction using bromobenzene and *p*-MeO-phenylboronic acid. To our surprise no cross-coupled product was observed with only homocoupled product observed, arising from homocoupling of *p*-MeO-phenylboronic acid, isolated in 9% yield.

Based on these data, a number of optimisation experiments were undertaken, as shown in Table 1, for the homocoupling of *para*-methoxyphenylboronic acid. In order to test the effect of the concentration of the Au catalyst on the reaction yield, 15 nm Au NPs–PEG_{10800} were used for the homocoupling of *p*-methoxyphenyl boronic acid in the presence of sodium hydroxide. The Au catalyst loading was varied (4.87, 6.25, 10, 25 and 50 μmol or 0.48, 0.62, 1, 2.5 and 5 mol%) and the isolated yield of the pure 4,4′-dimethoxybiphenyl product was found to be 6, 9, 25, 49 and 60% respectively (Fig. 4). Finally, to check the effect of the PEG length, Au NPs–PEG_{10800} were compared to the Au NPs–PEG_{20800} in the homocoupling reaction of *p*-methoxyphenylboronic acid and under similar conditions; our results did not show a big difference in the yield obtained of the pure products.

Stability in biological media and in the presence of biomolecules, Au NPs/cells interaction, and cytotoxicity

PEG–Au NPs were complexed with siRNA in order to test their toxicity in the presence and absence of siRNA. Due to the

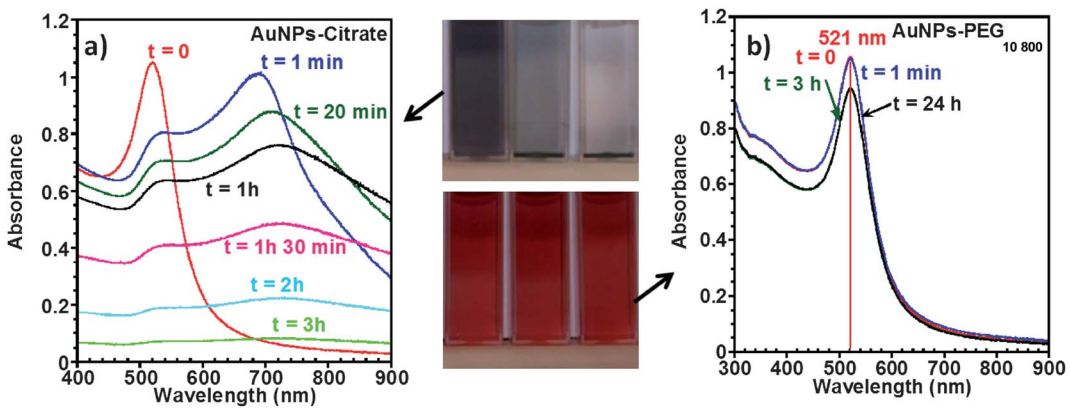

Fig. 2 Effect of salt (0.157 M NaCl) followed by UV-visible spectroscopy. (a) Au NPs–citrate, (b) Au NPs–PEG_{10800}. The pictures of the colloidal solutions in the middle show the high stability of the PEG–Au NPs colloidal solution in high ionic strength conditions, compared to Au NPs–citrate that are aggregated and precipitated.

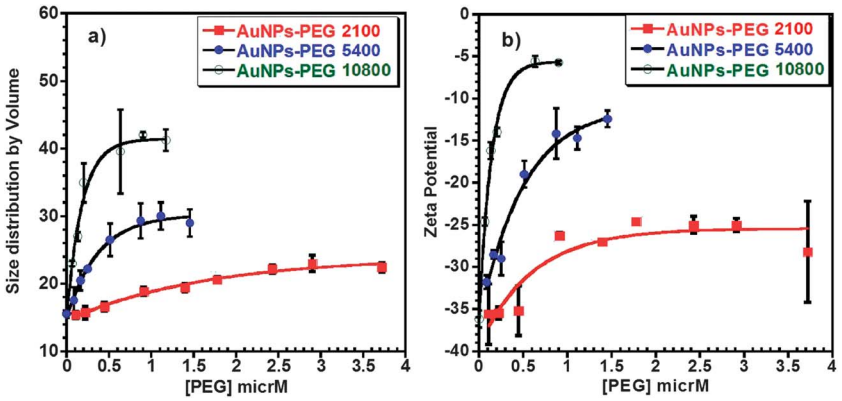

Fig. 3 (a) Size distribution by volume and zeta potential (b) of 15 nm Au NPs–PEG hybrids as a function of mPEG-SH polymer concentration expressed in μmol L^{-1}, for mPEG-SH with M_w 2100; 5400; and 10 800 g mol^{-1}.

anionic nature of the Au NPs, negatively charged naked siRNA would not readily bind to the particles. To allow binding, GL3 luciferase siRNA was first complexed with protamine (a positively charged peptide) at MR 5 producing complexes with an overall positive charge facilitating electrostatic interaction with the negatively charged nanoparticles. Zeta potential measurements showed an increase in charge from −1.9 ± 1.4 mV for siRNA alone, to 42 ± 1.15 mV when complexed with protamine. Complexes were produced with a range of Au NPs at MR 10 (Au:(siRNA:protamine)). These complexes exhibited a nearly neutral surface charge, and their sizes were slightly increased when compared to uncomplexed Au NPs (see Table S1†).

The viability of CT26 (ref. 39) and B16.F10 cells after treatment with the Au NPs was determined by the MTT assay. Cells were treated with a range of Au NPs complexed with protamine condensed siRNA at biologically active concentrations (Fig. 5). None of the PEG-coated Au nanoparticles synthesised in this study exhibited any cytotoxicity in B16.F10 or CT26 cell cultures, either alone or complexed with siRNA.[39] Association with cells is vital for NP-aided siRNA delivery. The protamine:siRNA complexation to the Au NPs does not have a significant effect on the toxicity of Au NPs. Protamine:siRNA on its own also does not exhibit any toxicity. The physical characteristics of the PEG–Au NPs were conserved after complexation with siRNA/protamine as no change in the colour of the colloidal solutions was observed after bioconjugation. However, a slight increase in the diameter of the 15 nm Au nanoparticles was observed after complexation with siRNA/protamine, as confirmed by DLS (Table S1†). The increase in the NP diameter was most likely due to weak interactions between neighbouring nanoparticles. However, this interaction was not strong enough to release the ligands from the surface of the NPs to allow direct core–core interaction.

Complexation with siRNA, characterization, and siRNA delivery

PEG–Au NPs were complexed with siRNA in order to test their usefulness as a delivery vector. Due to the anionic nature of the Au nanoparticles negatively charged, naked siRNA will not readily bind to the particles. To allow binding, GL3 luciferase siRNA was first complexed with protamine (a positively charged peptide) at MR 5 producing complexes with an overall positive charge facilitating electrostatic interaction with the negatively charged nanoparticles. Zeta potential measurements showed an increase in charge from −1.9 ± 1.4 mV for siRNA alone, to 42 ± 1.15 mV when complexed with protamine. Complexes were produced with a range of Au NPs at MR 10 (Au:(siRNA:protamine)). These complexes exhibited a positive surface charge, and their sizes were slightly increased when compared to uncomplexed Au NPs. For example, the 15 nm PEG_{2100} particles increased in size from 28 ± 1.5 nm (Table 1) to 46.95 ± 5.25 nm upon complexation of siRNA. A similar increase in size was noted when complexes were measured in transfection media (15 nm PEG_{2100} size increased to 138 ± 4.19). This increase was not, however, seen for larger Au NPs, *e.g.* the size of 30 nm PEG_{10800} was 72.8 ± 4 nm before complexation, 69.69 ± 0.5 nm

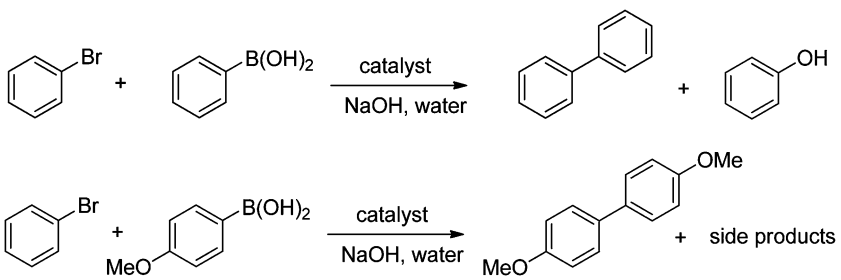

Scheme 1 Gold-catalyzed heterocoupling reaction of bromobenzene with phenylboronic acid or 4-methoxyphenylboronic acid.

Table 1 Homocoupling of MeO-PhB(OH)$_2$ whereby MeO-PhB(OH)$_2$ and PhBr were heated in the presence of NaOH and water

Boronic acid	PEG size	Base	Au size	Time/temp	Ratio of products by ^{1}H NMR: SM : homocoupled product : *p*MeO-phenol
MeO-PhB(OH)$_2$	10 800	NaOH	6 nm	80 °C/25 h	0 : 1 : 4.9
MeO-PhB(OH)$_2$	10 800	NaOH	30 nm	80 °C/25 h	0 : 1 : 10.3
MeO-PhB(OH)$_2$	10 800	NaOH	~60 nm	80 °C/25 h	1 : 1 : 23
MeO-PhB(OH)$_2$	5400	NaOH	15 nm	80 °C/25 h	0 : 1 : 4.7
MeO-PhB(OH)$_2$	20 800	NaOH	15 nm	80 °C/25 h	0 : 1 : 4.5
[a]MeO-PhB(OH)$_2$	20 800	Na_2CO_3	15 nm	80 °C/25 h	30 : 1 : 0
[b]MeO-PhB(OH)$_2$	20 800	Na_2CO_3	15 nm	80 °C/25 h	2.1 : 1 : 0.4
MeO-PhB(OH)$_2$	5400	Cs_2CO_3	15 nm	80 °C/20 h	4.6 : 1 : 7

[a] Solvent EtOH–water. [b] Solvent toluene.

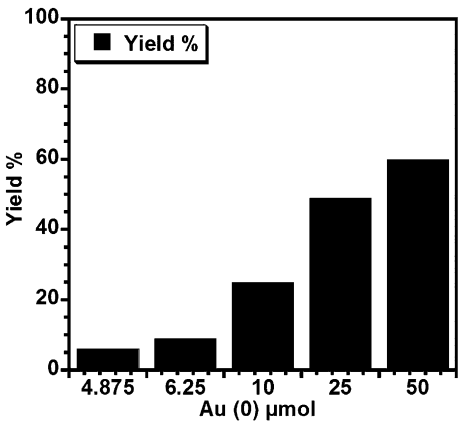

Fig. 4 Effect of catalyst concentration on the isolated yield for the homocoupling of *p*-methoxyphenyl boronic acid alone.

after siRNA complexation and 69.91 ± 0.6 nm when measured in transfection media. When assessing the loading of siRNA to cationic particles a gel retardation assay can be utilised.[41,42] This method cannot, however, be utilised in the case of protamine:siRNA binding to the Au particle as the complexation of the siRNA with protamine itself causes gel retardation and protects the siRNA from EtBr intercalation. Further studies to determine the extent of binding of the protamine:siRNA complex will be carried out in the future and these studies will include modified gel retardation assays and UV analysis of the complexes.

The association with cells is vital for NP-aided siRNA delivery.[43–45] The protamine:siRNA complexation to the Au NPs, as mentioned above, does not have a significant effect on the toxicity of the Au NPs. Protamine:siRNA on its own also does not exhibit any toxicity. In addition the protamine:siRNA complex at the MR used here does not display and knockdown effects when not complexed with Au NPs. The MR used was chosen as it introduces the charge change necessary for interaction with the Au NPs rather than for any inherent transfection effects. However, the siRNA–protamine loading used here is sufficient for transfection studies.[45] To examine this, fluorescent siRNA was complexed with PEG–Au nanoparticles as before, and their association with CT26 cells was assessed by fluorescence

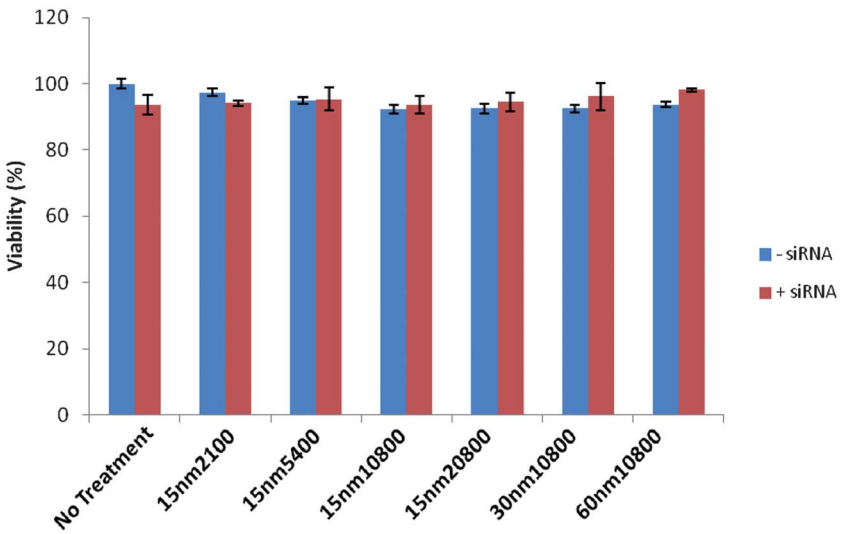

Fig. 5 Effect of Au–PEG complexes on B16.F10 cell viability. Cells were incubated with a range of Au–PEG:(siRNA:protamine) complexes or Au–PEG alone at a MR of 1 : 10 for 4 hours at 37 °C. A MTT assay was subsequently carried out and cell viability is expressed as % of dehydrogenase activity relative to untreated control.

microscopy (Fig. 6).[46,47] All of the tested Au NP formulations showed a good level of interaction, as evidenced by the green staining in the images (Fig. 6b–d). Protamine condensed siRNA alone showed negligible uptake (Fig. 6a) indicating the inability of siRNA alone to associate with cells. Transfection efficiency and gene silencing can be determined by measuring the reduction in the expression of a reporter gene, such as luciferase. GL3 luciferase siRNA was condensed with protamine and complexed with the PEG–Au nanoparticles. Knockdown in levels of luciferase protein expression[48] was seen with all of the PEG–Au complexes (30–50%) (Fig. 7) and significant knockdown, compared with the untreated control was seen with 4 particles; 15 nm-PEG_{2100}, 15 nm-PEG_{5400}, 30 nm-PEG_{10800} and 60 nm-PEG_{10800} ($p < 0.05$ – Student t-test). This compares favourably with the commercial siRNA delivery vector, Lipofectamine 2000, which achieved a knockdown of ~60%. No significant knockdown was observed with non silencing siRNA, confirming the specific nature of the siRNA. None of the PEG–Au NPs synthesised in this study exhibited any cytotoxicity in CT-26 cell cultures, either alone or when complexed with siRNA. The slightly negatively charged PEG–Au NPs produced in this study were able to interact electrostatically with protamine condensed fluorescent siRNA, allowing cellular association of the complexes to be monitored by fluorescence microscopy. The physical characteristics of the PEG–Au NPs were conserved after complexation with siRNA/protamine, as no change in the colour of the colloidal solutions was observed after bioconjugation.

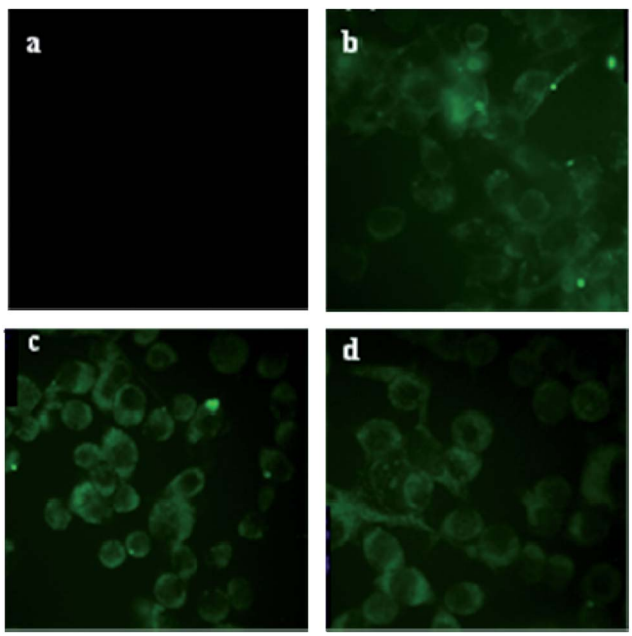

Fig. 6 Cellular association of Au NP–PEG complexed siRNA with CT26 assessed by fluorescent detection of labeled siRNA using a Nikon Eclipse TS100 inverted microscope equipped with fluorescein and DAPI filters and Metamorph version 6.1 software. Cells were treated (a) with protamine condensed siRNA (MR 1 : 5) alone (b) 15 nm Au NPs–PEG_{2100}:(protamine:siRNA), (c) 15 nm Au NPs–PEG_{5400}:(protamine:siRNA), (d) 60 nm Au NPs–PEG_{10800}:(protamine:siRNA). All Au NPs were complexed at a MR 10. 20 hours post transfection cells were fixed with PFA and stained with DAPI to visualise the nucleus.

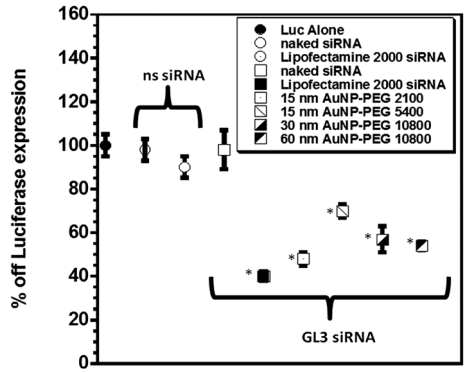

Fig. 7 siRNA knockdown of luciferase expression in CT26 cells with Au NPs. CT26 cells were transfected with pGL3 luciferase plasmid for 2 hours prior to treatment with GL3 siRNA complexed with Au NPs. Luciferase expression was determined 24 hours post siRNA transfection and is expressed as % of non-siRNA treated cells (results ± SEM of triplicate data) (*$p < 0.05$).

However, a slight increase in the size of the NPs after complexation with siRNA/protamine was detected by DLS, most likely due to weak interactions between neighboured nanoparticles; however, this interaction was not strong enough to release the ligands from the surface of the nanoparticles to allow direct core–core interaction. A net positive charge was measured for the Au NPs complexed with siRNA/protamine, making these suitable candidates for cellular delivery by interaction with the negatively charged plasma membrane. Data from cell association, as determined by fluorescence, and siRNA delivery, as determined by luciferase knockdown indicate that the particles are effective at associating with and entering cells.

Conclusions

Electrostatically-stabilised Au NPs–citrate have very limited applications due to their fast aggregation in complex media such as the presence of a high concentration of salts which is the main cause of this aggregation. However, steric stabilisation of Au NPs with PEG polymer offers a high degree of stability to the Au NPs dispersion. Au NPs–PEG hybrids were shown here to catalyse aryl homocoupling reactions in water, although no clear conversion was observed with 60 nm diameter NPs. The yield of the homocoupling reaction of *p*-methoxyphenyl boronic was found to increase with Au NPs–PEG loading, demonstrating the catalytic efficacy of the Au NPs–PEG in the catalytic homocoupling of boronic acids. Finally, all of the Au NP–PEG hybrids tested here were checked for cytotoxicity on B16.F10 and CT26 cell lines, and were found to be non-cytotoxic and able to deliver siRNA into the cells. Further studies to attach biomolecules on PEG–Au NPs and their interactions with platelets are now in progress in order to use these NPs in active targeting and receptor mediated delivery.

Acknowledgements

We acknowledge financial support from Science Foundation Ireland (Grant 07/SRC/B1155 and 07/SRC/B1154) to the Irish Drug

Delivery network (IDDN) through Strategic Research Cluster (SRC) grants. This research was also enabled by the Higher Education Authority Program for Research in Third Level Institutions (2007–2011) *via* the INSPIRE programme. Microscopy analysis was undertaken at the Electron Microscopy and Analysis Facility (EMAF) at the Tyndall National Institute, Cork, Ireland.

References

1 M. C. Daniel and D. Astruc, *Chem. Rev.*, 2004, **104**, 293–346.
2 A. Corma and H. Garcia, *Chem. Soc. Rev.*, 2008, **37**, 2096–2126.
3 B. I. Lee, L. Qi and T. Copeland, *J. Ceram. Process. Res.*, 2005, **6**, 31–40.
4 S. Link and M. A. El-Sayed, *J. Phys. Chem. B*, 1999, **103**, 4212–4217.
5 K. S. Lee and M. A. El-Sayed, *J. Phys. Chem. B*, 2006, **110**, 19220–19225.
6 Y. E. K. Lee and R. Kopelman, *Imaging and Spectroscopic Analysis of Living Cells: Optical and Spectroscopic Techniques*, Academic Press, UK, 2012, vol. 504, pp. 419–470.
7 P. Zrazhevskiy and X. Gao, *Miner. Biotechnol.*, 2009, **21**, 37–52.
8 S. K. Nune, P. Gunda, P. K. Thallapally, Y. Y. Lin, M. L. Forrest and C. J. Berkland, *Expert Opin. Drug Delivery*, 2009, **6**, 1175–1194.
9 R. M. Mohamed, D. L. McKinney and W. M. Sigmund, *Mater. Sci. Eng., R*, 2012, **73**, 1–13.
10 C. J. Murphy, T. K. San, A. M. Gole, C. J. Orendorff, J. X. Gao, L. Gou, S. E. Hunyadi and T. Li, *J. Phys. Chem. B*, 2005, **109**, 13857–13870.
11 C. J. Orendorff, T. K. Sau and C. J. Murphy, *Small*, 2006, **2**, 636–639.
12 K. Rahme, F. Gauffre, J. D. Marty, B. Payre and C. Mingotaud, *J. Phys. Chem. C*, 2007, **111**, 7273–7279.
13 R. A. Sperling, P. Rivera gil, F. Zhang, M. Zanella and W. J. Parak, *Chem. Soc. Rev.*, 2008, **37**, 1896–1908.
14 A. Abad, P. Conceptciòn, A. Corma and H. Garcia, *Angew. Chem., Int. Ed.*, 2005, **44**, 4066–4069.
15 D. I. Enache, J. K. Edwards, P. Landon, B. Solsona-Espriu, A. F. Carley, A. A. Herzing, M. Watanabe, C. J. Kiely, D. W. Knight and G. J. Hutchings, *Science*, 2006, **311**, 362–365.
16 H. Miyamura, R. Matsubara, Y. Miyazaki and S. Kobayashi, *Angew. Chem., Int. Ed.*, 2007, **46**, 4151–4154.
17 M. Haruta, N. Yamada, T. Kobayashi and S. Iijima, *J. Catal.*, 1989, **115**, 301–309.
18 J. Guzman and B. C. Gates, *J. Am. Chem. Soc.*, 2004, **126**, 2672–2673.
19 C. Lemire, R. Meyer, S. Shaikhutdino and H. J. Freund, *Angew. Chem., Int. Ed.*, 2004, **43**, 118–121.
20 A. Corma, *Science*, 2006, **313**, 332–334.
21 G. C. Bond, C. Louis and D. T. Thompson, *Catalysis by Gold*, Imperial College Press, 2006.
22 A. Arcadi and S. Di Giuseppe, *Curr. Org. Chem.*, 2004, **8**, 795–812.
23 A. S. K. Hashmi and G. H. Hutchings, *Angew. Chem., Int. Ed.*, 2006, **45**, 7896–7936.
24 J. Hamn, Y. Liu and R. Guo, *J. Am. Chem. Soc.*, 2009, **131**, 2060–2061.
25 B. Karimi and F. K. Esfahani, *Chem. Commun.*, 2011, **47**, 10452–10454.
26 S. Carrettin, J. Guzman and A. Corma, *Angew. Chem., Int. Ed.*, 2005, **44**, 2242–2245.
27 Y. J. Liang, M. Ozawa and A. Krueger, *ACS Nano*, 2009, **3**, 2288–2296.
28 I. Romer, T. A. White, M. Baalousha, K. Chipman, M. R. Viant and J. R. Lead, *J. Chromatogr., A*, 2011, **1218**, 4226–4233.
29 K. Rahme, P. Vicendo, C. Ayela, C. Gaillard, B. Payre, C. Mingotaud and F. Gauffre, *Chem.–Eur. J.*, 2009, **15**, 11151–11159.
30 H. Otsuka, Y. Nagasaki and K. Kataoka, *Adv. Drug Delivery Rev.*, 2003, **55**, 403–419.
31 J. Rubio-Garcia, Y. Coppel, P. Lecante, C. Mingotaud, B. Chaudret, F. Gauffre and M. L. Kahn, *Chem. Commun.*, 2011, **47**, 988–990.
32 F. Ullmann and J. Bielecki, *Ber. Dtsch. Chem. Ges.*, 1901, **34**, 2174–2185.
33 D. A. Horton, G. T. Bourne and M. L. Smythe, *Chem. Rev.*, 2003, **103**, 893–930.
34 D. A. Fleming and M. E. Williams, *Langmuir*, 2004, **20**, 3021–3023.
35 G. Frens, *Nature (London), Phys. Sci.*, 1973, **241**, 20–22.
36 J. Kimling, M. Maier, B. Okenve, V. Kotaidis, H. Ballot and A. Plech, *J. Phys. Chem. B*, 2006, **110**, 15700–15707.
37 J. Turkevich, P. C. Stevenson and J. Hillier, *Discuss. Faraday Soc.*, 1951, **11**, 55–75.
38 S. Sistach, K. Rahme, N. Perignon, J. D. Marty, N. L. D. Viguerie, F. Gauffre and C. Mingotaud, *Chem. Mater.*, 2008, **20**, 1221–1223.
39 K. Rahme, L. Chen, R. G. Hobbs, M. A. Morris, C. O'Driscoll and J. D. Holmes, *RSC Adv.*, 2013, **3**, 6085–6094.
40 K. Rahme, J. Oberdisse, R. Schweins, C. Gaillard, J. D. Marty, C. Mingotaud and F. Gauffre, *ChemPhysChem*, 2008, **9**, 2230–2236.
41 M. S. Suh, G. Shim, H. Y. Lee, S.-E. Han, Y.-H. Yu, Y. Choi, K. Kim, I. C. Kwon, K. Y. Weon, Y. B. Kim and Y.-K. Oh, *J. Controlled Release*, 2009, **140**, 268–276.
42 Y. H. Yu, E. Kim, D. E. Park, G. Shim, S. Lee, Y. B. Kim, C.-W. Kim and Y.-K. Oh, *Eur. J. Pharm. Biopharm.*, 2012, **80**, 268–273.
43 X.-Z. Yang, S. Dou, T.-M. Sun, C.-Q. Mao, H.-X. Wang and J. Wang, *J. Controlled Release*, 2011, **156**, 203–211.
44 J. Zhou, K.-T. Shum, J. C. Burnett and J. J. Rossi, *Pharmaceuticals*, 2013, **6**, 85–107.
45 P. Guo, O. Coban, N. M. Snead, J. Trebley, S. Hoeprich, S. Guo and Y. Shu, *Adv. Drug Delivery Rev.*, 2010, **62**, 650–666.
46 V. Sée, P. Free, Y. Cesbron, P. Nativo, U. Shaheen, D. J. Rigden, D. G. Spiller, D. G. Fernig, M. R. H. White, I. A. Prior, M. Brust, B. Lounis and R. Lévy, *ACS Nano*, 2009, **3**, 2461–2468.
47 R. Lévy, U. Shaheen, Y. Cesbron and V. Sée, *Nano Rev.*, 2010, **1**, 4889–4907.
48 Y. Kamachi, Y. Okuda and H. Kondoh, *genesis*, 2008, **46**, 1–7.

